PCCP
Physical Chemistry Chemical Physics

Accepted Manuscript

This article can be cited before page numbers have been issued, to do this please use: M. Chaudhary, T. K. Panda and S. K. Singh, *Phys. Chem. Chem. Phys.*, 2025, DOI: 10.1039/D5CP02589C.

View Article Online
DOI: 10.1039/D5CP02589C

Mechanistic Insights into Neosilyllithium-Catalyzed Hydroboration of Nitriles, Aldehydes, and Esters: A DLPNO-CCSD(T) Study

Mridula Choudhary[a], Tarun K. Panda[b]* and Saurabh Kumar Singh[a]*

[a]Computational Inorganic Chemistry Group, Department of Chemistry, Indian Institute of Technology Hyderabad, Kandi, Sangareddy, Telangana-502284, India. Email: sksingh@chy.iith.ac.in

[b]Synthetic Organometallic Chemistry and Catalysis lab, Indian Institute of Technology Hyderabad, Kandi, Sangareddy, Telangana-502284, India. Email: tpanda@chy.iith.ac.in

View Article Online
DOI: 10.1039/D5CP02589C

Abstract

Over the past few years, alkali and alkaline earth metals have emerged as alternative catalysts for transition metal organometallics to catalyze the hydroboration of unsaturated compounds. A highly selective and cost-effective lithium-catalyzed method for the synthesis of an organoborane has been established based on the addition of a B-H bond to an unsaturated bond (polarized or unpolarized) using pinacolborane (HBPin). In the present work, the neosilyllithium-catalyzed hydroboration of nitrile, aldehyde, and ester has been investigated using high-level DLPNO-CCSD(T) calculations to unravel the mechanistic pathways and substrate-dependent reactivity. Using non-covalent interaction (NCI), intrinsic bond orbital (IBO), and activation strain analysis (ASA), we thoroughly analyzed the nature of key intermediates and transition states. DLPNO-CCSD(T) study reveals that the initial interaction between neosilyllithium and pinacolborane forms a stable zwitterionic intermediate, which polarizes the B–H bond and enables efficient hydride transfer. Specifically, the hydroboration of nitriles involves two sequential hydride transfers, where the first reduction of nitrile to imine occurs via a six-membered transition state, with a huge free energy barrier of ~15 kcal/mol, while the second step with imine-to-amine reduction proceeds with a tiny barrier of ~3.1 kcal/mol. ASA analysis of the transition state suggests that the linear geometry of the nitrile group incurs a significant distortion penalty compared to the pre-bent imine geometry, making the second hydride transfer much facile in nature. The hydroboration aldehydes require a moderate free energy barrier for the hydride transfer barrier (~8.3 kcal/mol), and the desired products are thermodynamically stable. On the other hand, for esters, the computed Gibbs free energy profile displays a notably higher activation barrier (~17.5 kcal/mol), compared to aldehydes, which agrees with experimental observations that the hydroboration of esters is more challenging. A significant steric hindrance surrounding the ester functional group has been demonstrated to markedly augment the strain energy during the hydride transfer step, engendering a higher activation energy barrier for esters compared to aldehydes. Our findings suggest an interplay of steric and electronic factors in dictating substrate reactivity and the dual role of HBPin as both a hydride donor and functional group acceptor in neosilyllithium-catalysed hydroboration reaction.

View Article Online
DOI: 10.1039/D5CP02589C

Introduction

The hydroboration reaction, which involves the insertion of a B-H bond to an unsaturated chemical group, is a valuable and atom-efficient method for synthesizing organoboranes. This pioneering reaction was first described by H.C. Brown in 1956, marking a significant advancement in hydroboration chemistry, leading to the Nobel Prize in 1979.[1] Organoboranes play a vital role as synthetic intermediates across a wide range of organic reactions, as they can be readily transformed into various other functionalities with relative ease and high yields. While early research was focused on transforming organoboranes into the corresponding alcohols,[2,3] the development of additional transformations, particularly the Suzuki-Miyaura cross-coupling reaction for carbon-carbon bond formation, has significantly increased the role of organoboranes in organic synthesis.[5,6] Traditionally, classical hydride reagents[7–9] or high-pressure hydrogenation[10] were required to reduce polarized multiple bonds like esters or nitriles, but these reagents can lead to poor selectivity and harsh conditions. Catalytic hydroboration using pinacolborane (HBPin) or catecholborane (HBcat) as a mild hydroborating agent has gained significant attention as a more chemoselective and functional-group-tolerant reduction method. In a seminal discovery, Kono and Ito *et al.* reported the first observation of the metal-catalyzed hydroboration of alkenes where the HBcat underwent oxidative addition with the rhodium-catalyzed Wilkinson's catalyst to yield the hydroborated product.[11] Later, Männing and Nöth *et al.* extended these studies to alkynes.[12] Since then, there has been a remarkable and exponential increase in designing transition metal and lanthanide-based catalysts for chemoselective and regioselective hydroboration.[13–18] These metal catalysts are highly effective and selective in the hydroboration of polarised and unpolarised bonds. Despite their effectiveness, catalytic conversion using these metal catalysts is expensive and potentially toxic (Rh, Ir, etc.), as well as the need for rigorously inert conditions, making them less appealing to large-scale industrial applications, particularly in the pharmaceutical and material synthesis fields where residual transition metals must be precluded. Hence, replacing expensive and toxic transition metals with earth-abundant, non-toxic, and cost-effective alkali and alkaline earth metals is highly desirable to address these challenges.[19] This motivated researchers to study main-group-catalyzed hydroboration as a sustainable alternative.[20,21] Organometallic complexes derived from early main group elements exhibit high reactivity, strong

Brønsted basicity, and nucleophilicity, making them highly effective polar reagents and promising catalysts for various organic transformations.[19] Among these, alkaline earth metals have been extensively studied for the catalytic hydroboration of polar bonds, including amides, esters, ketones, imines, and aldehydes, as they offer significant advantages, such as abundance, low toxicity, and efficient activation of these substrates.[17–24] A significant breakthrough was achieved in 2019 by Rupeing and co-workers, who reported the first hydroboration of internal and terminal alkynes (non-polarized C≡C bonds) using a $MgBu_2$ catalyst[29] and showcasing the potential of group II metals to go beyond conventional hydroboration of polar bonds, highlighting their broader applicability in catalytic processes involving both polar and non-polar substrates. These systems often operate via a σ-bond metathesis mechanism, wherein a metal-alkyl species exchanges with the B–H bond of HBPin, forming a metal–hydride intermediate that delivers hydride to the substrate, followed by regeneration via another metathesis step.[23,30–34] This cycle proceeds without a change in the metal oxidation state, making it ideal for redox-inert main group metals. In the last decade, much attention has been shifted towards alkali metals (Li, Na, K) for hydroelementation reactions[35], and lithium compounds, in particular, are undoubtedly a good choice due to their inexpensiveness and commercial availability. A notable breakthrough in this area was reported by Okuda and co-workers in 2016, who employed a series of lithium, sodium, and potassium hydridophenylborate, for the selective hydroboration of benzophenone as a model substrate.[36] Their findings revealed that the lithium complex displayed superior catalytic activity compared to its sodium and potassium analogues, owing to the higher degree of polarization. In 2018, Sen et al. reported that three readily accessible lithium compounds, 1,1-dilithioferrocene, 2,6-di-tert-butyl phenolate lithium, and *β*-diketiminate lithium, towards the facile hydroboration of a wide range of aldehydes and ketones, using HBPin.[37] Subsequently, Xue and co-workers reported n-BuLi as a competent catalyst for the hydroboration of imines and nitriles. Control experiments, combined with density functional theory (DFT) calculations by Zhu *et al.* (2018) suggested that n-BuLi first reacts with HBPin to form a lithium-borate complex, which unveils the key step in initiating the reaction.[38] In recent years, lithium-based catalysts have gained significant attention for their versatility in various catalytic reactions, including hydrogenation[39], oxidative dehydrogenation[40], polymerization[41], carbon-carbon bond formation[42] , hydrosilylation, hydroboration, and many others[35]. Collectively, these studies have

View Article Online
DOI: 10.1039/D5CP02589C

triggered a renaissance in lithium chemistry and reaffirmed the pivotal role of lithium-based compounds as efficient catalysts in various catalytic transformations.

Recently, Panda and co-workers have reported hydroboration of alkenes, alkynes, organic nitriles, carboxylic esters, and carboxamides with HBPin using an alkali metal catalyst, neosilyllithium ($LiCH_2SiMe_3$), at room temperature and solvent-free conditions, which offered a high yield of the corresponding borylated products[43,44] Control experiments and density functional theory (DFT) calculations of both studies suggest that the neosilyllithium binds HBPin and then undergoes a nucleophilic attack, generating a borate intermediate (zwitterionic species), which aids the hydride transfer to the substrate via the formation of a six-membered ring transition state. Previous experimental findings suggest that nitriles undergo facile double hydroboration, yielding 1,1-diborylamines in excellent yield, whereas ester hydroboration differs from other carbonyl compounds as it often yields a mixture of alcohol. This is due to its two-step reduction: first to aldehyde, then to alcohol, with each step potentially proceeding at different rates.

In the present manuscript, we have considered neosillylithium-catalyzed hydroboration reactions as our template and developed mechanistic insight into the hydroboration of nitrile, aldehyde, and ester by computing the reaction profile at DLPNO-CCSD(T) (domain-based local-pair natural orbital coupled cluster singles doubles with perturbative triples contribution) level of theory. We computed the relative Gibbs free energies at the DLPNO-CCSD(T)/def2-TZVP//M06/6-31G** functional level. Here, we opted for three distinct substrates: phenyl nitrile (**D**), benzaldehyde (**E**), and methyl benzoate (**F**) to elucidate the mechanistic insight and distinct reactivity differences that dictate selectivity and efficiency of the C≡N and C=O double bonds, where the former one is a triple bond. To rationalize these differences, we performed an in-depth mechanistic analysis using Intrinsic Bond Orbital (IBO), Natural Bond Orbital (NBO), and Activation Strain Analysis (ASA) analyses to show how the geometric, electronic, and steric factors control the hydroboration of substrates **D**-**F**. Although all three substrates contain polarized π-bonds, their reactivity profiles under neosilyllithium catalysis differ markedly. Employing geometrical, orbital, and distortion/interaction analysis, we aim to comprehend the differences in activation barriers among various pathways. We believe that our in-depth computational study provides valuable insights into the underlying mechanistic details.

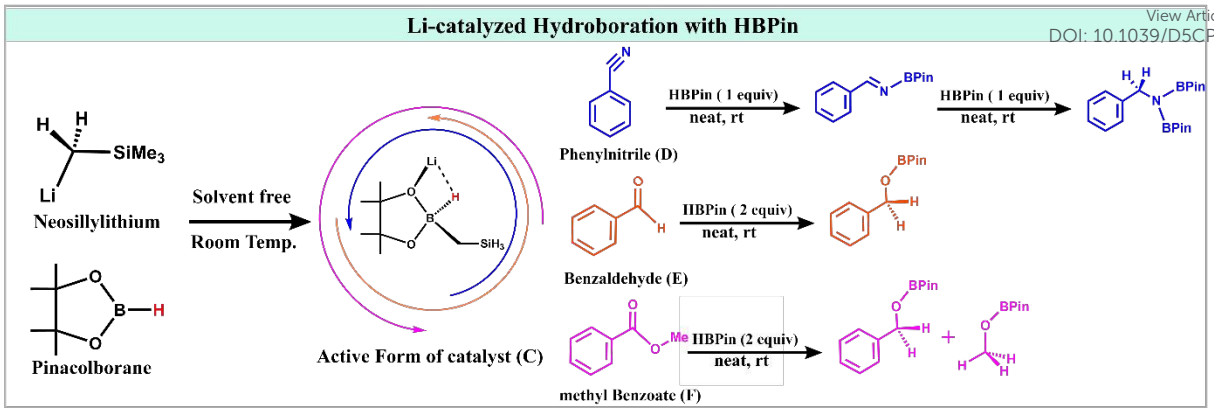

Scheme 1. Neosilyllithium catalyzed hydroboration using HBPin for phenyl nitrile (D), benzaldehyde (E), and methyl benzoate (F).

View Article Online
DOI: 10.1039/D5CP02589C

Computational Methodology

Density functional theory (DFT) calculations were carried out using the Gaussian 09 code.[45] Geometry optimizations were performed using the Minnesota M06 functional [46–48] and the Pople's split-valence double zeta 6-31G** basis set [49–51] for all the atoms. All the geometry optimization was carried out in the gas phase, as no solvent was included in the experimental setup. The optimized geometries were verified as stationary points on the potential energy surface by evaluating their vibrational frequencies. Transition states (TS) were characterized by exhibiting exactly one imaginary frequency corresponding to the reaction coordinate. We computed all the thermodynamic contributions to the energy, enthalpy, and free energy at the same level of theory at 1 atm and 298.15 K. To further ascertain the correctness of the TS, intrinsic reaction coordinate (IRC)[52–54] calculations were performed, which ensured that each transition state connected the correct forward and backward minima. Single-point calculations were carried out at DLPNO-CCSD(T)[55–57]/def2-TZVPP[58] level of theory on the DFT optimized geometries using ORCA 5.0.4 code.[59] All the DLPNO energies were obtained using "TightPNO" and "verytightSCF" settings. We have used the resolution-of-the-identity (RI) approach in the SCF part for both the Coulomb and the exchange terms (RIJK). Natural Bonding Orbital (NBO)[55] analysis was carried out using Weinhold's NBO 3.1 code12 as implemented in Gaussian 09. The three-dimensional molecular orbitals and optimized structures were visualized using the ChemCraft program. IBO analysis was performed using the IBOview software to visualize electron flow along reaction paths.[60] The non-covalent interaction (NCI) analysis was carried out using the Multiwfn code [61] and visualized through VMD [62]. Additionally, we applied the Activation Strain Analysis (ASA) using Pyfrag 2019 [63–65] as implemented in Gaussian 09 to investigate the relationship between activation barriers and the structural and electronic characteristics of catalysts and substrates. In this model, the Potential energy surface $\Delta E(\zeta)$ along the reaction coordinates ζ is decomposed into two contributions: the distortion energy $\Delta E_{dist}(\zeta)$, associated with the structural changes required to reach the transition state, and the interaction energy $\Delta E_{int}(\zeta)$, which accounts for the interactions between distorted reactants. This relationship is expressed as shown in Equation (1):

$$\Delta E(\zeta) = \Delta E_{dist}(\zeta) + \Delta E_{int}(\zeta) \qquad (1)$$

View Article Online
DOI: 10.1039/D5CP02589C

Results and Discussion

Before we delve into the mechanistic insights into the neosilyllithium-mediated hydroboration reactions using phenyl nitrile (**D**), benzaldehyde (**E**), and methyl benzoate (**F**), we have first explored the role of the hydroborating agent (HBPin) in the hydroboration reactions. The chemistry of HBPin is fascinating as it is capable of performing hydroboration in the absence of any solvent or external catalyst.[66,67] The presence of two B-O bonds in the HBPin stabilizes the positive charge on the B atom upon the transfer of hydride, which is a key feature for facile hydride transfer. Here, we first analyzed the hydroboration of the substrates **D** and **E** directly using only the HBPin. DFT calculations predict adduct formation through weak van der Waals interactions between substrate **D**(**E**) and HBPin, which is 8.1(5.6) kcal/mol higher in energy than the non-interacting species as shown in Fig.1. In the subsequent step, the adduct undergoes a four-membered transition state where the N(O) atom of substrate **D**(**E**) attacks the boron atom of HBPin and simultaneously hydride transfer occurs from HBPin to the carbon atom of substrate **D(E),** resulting in the desired hydroborated product. The Gibbs free energy barrier for this four-membered TS is ~49.9 (41.5) kcal/mol, which is significantly uphill for the conversion to occur at room temperature. This high-energy TS agrees with the experimental observation where ^{1}H NMR shows no reaction after 24 hours at room temperature between HBPin and substrates **D** and **E**.[43] DFT calculations predict that the neat HBPin can offer hydroboration of nitriles/aldehydes in the absence of any catalyst; however, facile hydroboration at room temperature requires the addition of the catalyst along with HBPin to overcome the giant activation barrier.

View Article Online
DOI: 10.1039/D5CP02589C

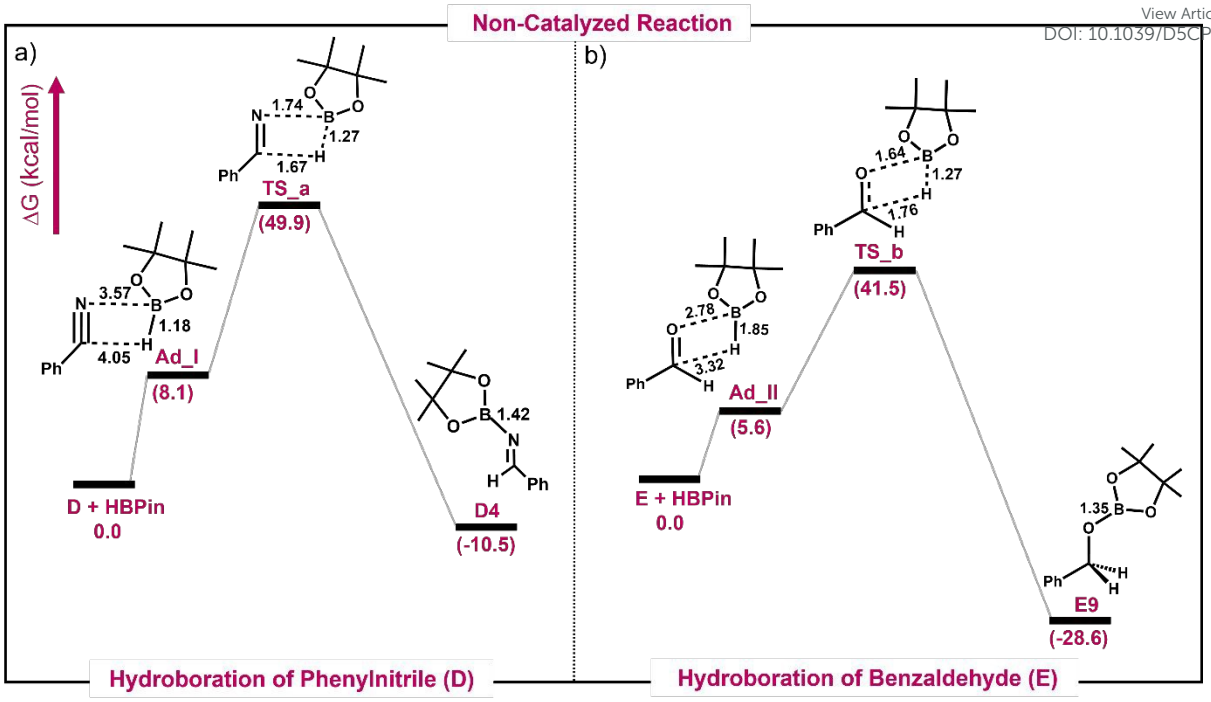

Fig. 1: DLPNO-CCSD(T)/def2-TZVPP//M06/6-31G** computed relative Gibbs free energy for hydroboration of the phenyl nitrile(D)/benzaldehyde (E) using HBPin and without any external catalyst. The relevant bond distances are provided in Å.

Interaction of neosilyllithium with HBPin: Formation of the active form of the catalyst

It is evident from the DFT calculations that the hydroboration of phenyl nitrile **(D)** and benzaldehyde **(E)** only with HBPin is subjected to a high energy barrier that cannot be surmounted at room temperature. To significantly reduce the computational cost, we employed a truncated model of neosilyllithium, replacing Li-CH_2-$Si(CH_3)_3$ with Li-CH_2-SiH_3. In th first step, the HBPin binds with the $LiCH_2SiH_3$ catalyst, resulting in the formation of species **A**, which is stabilized by ~9.1 kcal/mol compared to the non-interacting species (see Fig. 2a). A strong electrostatic interaction between the positively charged Li atom and electronegative O atom of the HBPin favours the formation of Li-O bond in species **A**. (see Fig. S1a) The structural parameters of intermediate **A** indicate a Li–O bond length of 1.934 Å and a Li–CH_2SiH_3 bond length of 1.993 Å, where the latter bond length is slightly elongated compared to non-interacting species. In the next step, an intramolecular rearrangement takes place wherein the elongated Li-CH_2SiH_3 bond breaks, and the -CH_2SiH_3 group migrates to the boron atom of the HBPin through a four-membered transition state **TS1**. This process has a free energy barrier of ~ 9.8 kcal/mol, which results in the formation of zwitterionic intermediate **B**. This step is exergonic, where intermediate **B** is stabilized by ~ 7.6 kcal/mol than **A**. Intrinsic bond orbital (IBO) analysis of **TS1** (see Fig. 2b) suggests that the lone pair of the -CH_2SiH_3 group moves to the vacant orbital of the boron atom of HBPin, resulting in the tetracoordinated boron centre of the HBPin. Second-order perturbation analysis of **TS1** reveals a -32.6 kcal/mol interaction between the $2p_x$ orbital of the carbon atom in the silyl methyl group and the vacant $\sigma^*(2p_x - 2p_x)$ orbital in the B–O bond (90%B + 10%O) (see Fig. 2c). Next, intermediate **B** undergoes conformational change where the B-H bond aligns, comes close to the Li atom via low activation energy barrier **TS2** (~ 3.1 kcal/mol), and forms an intermediate **C** that is further stabilized by ~6.0 kcal/mol compared to the species **B**. Structural parameters of intermediate **C** suggest that the B-O-Li-H atoms come in one plane and form a four-membered ring with the formation of the Li-H bond of 1.771 Å. (see Fig. 2d). Although the four-membered rings are highly strained, the increased stability is associated with the strong donor-acceptor interaction between the B-H bond pair and vacant 2s orbital of the Li atom. Natural population analysis (NPA) of intermediate **C** reveals an increase in the B-H bond polarity compared to free HBPin, with a significant positive charge of +0.661 a.u. on the boron atom and –0.235 a.u. on the hydrogen atom, indicating

View Article Online
DOI: 10.1039/D5CP02589C

binding of the neosilyllithium aids in enhancing the hydricity of the H atom which plays a key role in facilitating the hydride transfer (see Table S1). An exergonic formation of the zwitterionic intermediate **C** represents the most active form of the catalyst, which further interacts with different substrates for the hydroboration reaction. The energy of the intermediate **C** will be considered as the reference for the hydroboration reactions. To validate the reaction profile computed using the truncated model complex, we recalculated the active form of the catalyst using the neosilyllithium complex (Li-CH_2-Si(CH_3)$_3$). The computed reaction profile with the original catalyst closely matches the truncated model complex, demonstrating that our truncated model mimics the original catalyst (see Fig. S3). To further check the possibility of the formation of alkali metal hydride LiH as a possible catalyst for the hydroboration reactions, we computed the dissociation of species **C** in LiH and BCH_2SiH_3 species. The computed reaction profile suggests that the dissociation of species **C** in LiH and BCH_2SiH_3 species is both thermodynamically and kinetically unfavourable, hence eliminating the possibility of the bimolecular-assisted process being a competitive pathway through formation of LiH for hydroboration (see Fig. S4)[68].

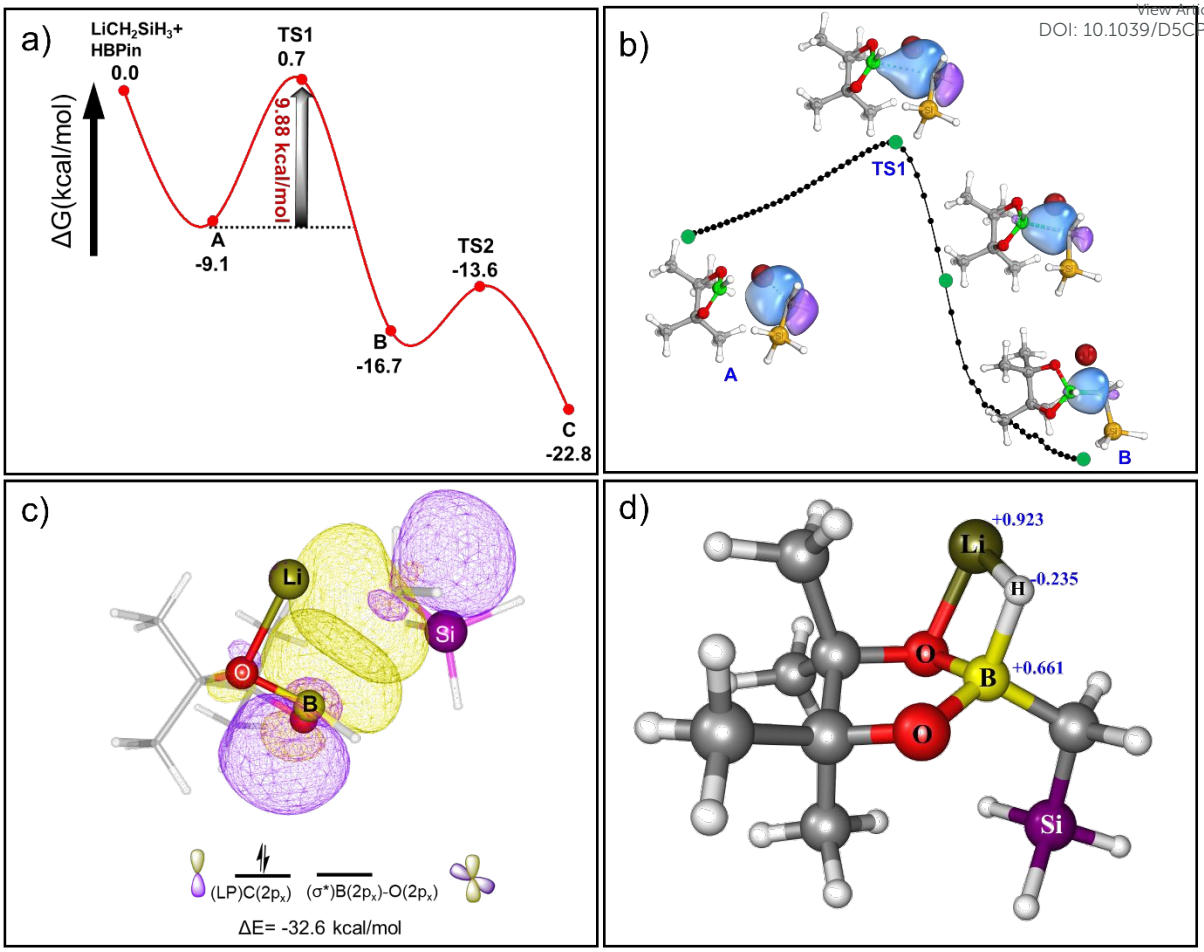

Fig. 2: **a)** DLPNO-CCSD(T)/def2-TZVPP//M06/6-31G** computed relative Gibbs free energy profile for generating a catalytically active species C from $LiCH_2SiH_3$+ HBPin. The relative free energy of each intermediate and transition state is given in kcal/mol. **b)** Changes of the intrinsic bond orbital (IBO) during B-C bond formation along the selected intrinsic reaction coordinates (IRCs). Color code : B(Green), Si (Yellow), O(Red), Li(Dark Red), C(Grey), H(white). **c)** NBO represents the most stabilizing interaction in the **TS1**. Δ*E* here represents donor-acceptor interactions obtained from second-order perturbation analysis**. d)** The optimized structure of the active form of the catalyst (C) along with the corresponding NPA charges on key atoms.

Hydroboration of Nitriles

Here, we have chosen phenyl nitrile (**D**) as the substrate for modelling the hydroboration of nitriles. (see Fig. 3 and Fig. 4) In the first step, substrate **D** interacts with species **C** and forms an intermediate **D1**, where a weak Li-N bond (2.061 Å) has been formed. The binding of phenyl nitrile with catalyst **C** is an exergonic process, where species **D1** is ~ 4.9 kcal/mol lower in energy than the unreacted species. In the next step, the B-H breaks via **TS3**, and hydride transfer occurs from the B atom to the sp-

View Article Online
DOI: 10.1039/D5CP02589C

hybridized carbon atom of the phenyl nitrile, forming an imino phenyl species **D2**. In **TS3**, two key transformations occur simultaneously, where the first B–H bond elongates from 1.251 Å (**D1**) to 1.341 Å (**TS3**) as a result of the hydride transfer to the sp-hybridized carbon atom of the nitrile group, at the same time, the Li-N bond gets stronger as the bond length decreases from 2.061 Å (**D1**) to 1.901 Å (**TS3**). Moreover, the Li-N bond becomes much shorter in **D2** (1.771 Å) compared to **D1,** which indicates that the binding of iminophenyl species with the Li atom is stronger than that of nitrile. This hydride transfer occurs via a six-membered transition state, **TS3,** with a free energy barrier of ~15 kcal/mol, which is the rate-determining step for the reaction. Intrinsic Reaction Coordinate (IRC) calculations confirm that **TS3** connects the pre- and post-hydride transfer intermediates, validating its role in the catalytic cycle. (see Fig. S9) Natural Bond Orbital (NBO) analysis of **TS3** reveals a significant donor-acceptor interaction (~55.6 kcal/mol) from the 1s orbital of the hydrogen atom to the vacant π antibonding orbital of C-N, consistent with the formation of the C–H bond and elongation of the C-N bond in **D2** compared to species **D1**. (See Fig. S5) In the next step, the iminophenyl species migrates by breaking the Li-N bond to the boron center and forming a highly stable zwitterionic species **D3,** which is stabilized by ~16.9 kcal/mol compared to **D2**. During the **D2 → TS4 → D3,** we observed a donor-acceptor interaction of ~32 kcal/mol from the 2s orbital of the nitrogen atom to the vacant $2p_z$ orbital of the B atom, resulting in the formation of the B-N bond. Subsequently, the ligand exchange step takes place, where the imine group attached to the boron center is flushed with the addition of the HBPin, facilitating the detachment of the borylimine product (**D4**) and regeneration of the catalyst **C** for the subsequent cycle. Overall, our calculations predict that the hydride transfer occurs through the six-membered transition state **TS3** is a rate-determining step that requires an energy barrier of ~15 kcal/mol for the conversion of phenyl nitrile (**D**) to the borylimine product (**D4**), which is significantly smaller than the giant barrier height ~49 kcal/mol observed for the HBPin mediated hydride transfer without any catalyst. NBO charge analysis of **TS_a** and **TS3** reveals that the hydride atom of the HBPin bears a charge of –0.009 a.u. in **TS_a,** while the formation of the zwitterionic species in **TS3** poses a giant negative charge of –0.10 a.u. on the hydride atom, demonstrating the ability of the neosilyllithium in polarizing and increasing the hydricity of the B-H bond, which facilitates the smooth hydride transfer to the carbon atom of phenyl nitrile. Overall, the presence of neosilyllithium catalyst helps in increasing

View Article Online
DOI: 10.1039/D5CP02589C

the hydricity of the B-H bond, which explains the role of the neosilyllithium catalyst in the hydroboration reaction.

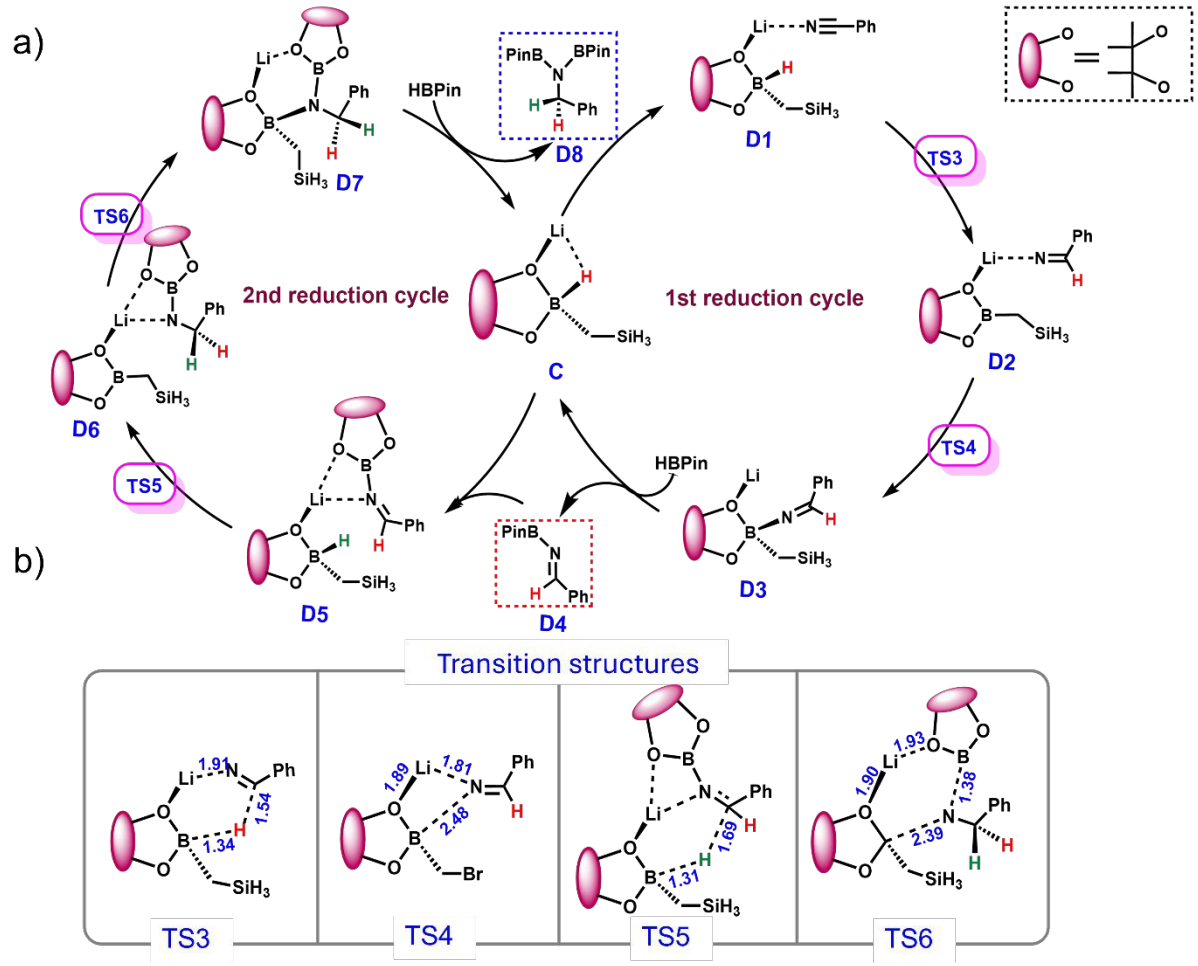

Fig. 3 **a)** Proposed catalytic cycle for neosilyllithium-catalyzed dihydroboration of phenyl nitrile (D) **b)** Transition structures with important hydrogen atoms shown for clarity. Bond lengths (in blue) are given in Å.

The ^{1}H NMR analysis of the reaction mixtures yielded diborylamine (**D8**) as the final product, which suggests that the double hydroboration (i.e., from nitrile→imine→amine) occurs during the reaction.[43] In addition, previous studies also suggest that, unlike aldehydes and esters, where monohydroborated products are obtained, these nitriles undergo stepwise reduction where the first B–H addition to yield a reactive imine, which undergoes a second hydride transfer to form the desired 1,1-diborylamines.([43,69–72]) The second reduction cycle started where the borylimine product (**D4**) from the first reduction cycle further binds with the regenerated catalyst **C** to form **D5,** similarly to how nitrile binds to the Li atom. Notably, the binding of borylimine product (**D4**) with catalyst **C** shows marginal stabilization of ~1 kcal/mol compared to the intermediate (**D1**), which is stabilized by ~4 kcal/mol. In the next step, the

View Article Online
DOI: 10.1039/D5CP02589C

hydride transfer step **(TS5)** occurs via the six-membered transition state and generates aminophenyl species **D6.** Notably, this hydride transfer occurs through a very low-energy barrier transition state **TS5** (~3.1 kcal/mol), which is ~5x times smaller than the energy barrier observed for **TS3**. Contrary to the endergonic hydride transfer for nitrile reduction, the **D5→TS5→D6** transformation is a highly exergonic process where the aminophenyl species **D6** is stabilized by ~35 kcal/mol compared to **D5**. The computed free energy profile suggests that the second reduction product is thermodynamically and kinetically favourable compared to the nitrile reduction. To elucidate the origin of the substrate-dependent reactivity in hydroboration, we performed Activation Strain Analysis (ASA) analysis on the key transition states involved in the hydride transfer to nitrile (**TS3**) and imine (**TS5**) (see Fig. S7). It is evident from Fig. S7 that the C≡N triple bond in phenylnitrile requires a substantial geometric reorganization cost to adopt the bent transition-state geometry (**TS3**), which results in the giant strain cost of 15.3 kcal/mol. Contrarily, a much smaller strain energy of ~ 2.1 kcal/mol is required for the imine to opt for the **TS5** configuration. On the other hand, **TS3** benefits from stronger stabilizing interactions (ΔE_{int} = –4.2 kcal/mol) than the **TS5** (–1.2 kcal mol^{-1}), however, these interactions are insufficient to compensate for the substantial strain contribution in the **TS3**. Hence a remarkably higher barrier observed for nitrile hydroboration ($\Delta G^{\ddagger}$ = *15 kcal/mol*) compared to imine ($\Delta G^{\ddagger}$ = *3.1 kcal/mol*) is primarily attributed to a significantly large distortion energy (ΔE_{dist}) during the hydride transfer step in **TS3**. Next, as observed in the first cycle, the amino phenyl species also migrates to the boron center via a six-membered transition state (**TS6),** forming the **D7** intermediate. This step has an activation barrier of ~6.7 kcal/mol. In the final step, the ligand exchange step takes place where the amino phenyl group attached to the boron center is flushed with HBPin and releases the desired $PhCH_2N(BPin)_2$ product **(D8)**, and regenerates the active catalyst **(C)** for the next subsequent cycle. Our calculations show that the reaction of the HBPin with one equivalent of the neosillyllithium would generate the active form of the catalyst, which later interacts with the substrate and facilitates the hydride transfer to generate the desired product. Later, another equivalent of HBPin helps release the product and regenerates the catalyst for the next cycle. A similar scenario occurs for the second reduction cycle, where borylimine gets reduced to diborylamine as the final product; however, a weaker C-N bond strength, more accessible imino-N lone pair, and lower strain energy enable easier activation through a

tiny barrier height (~3.1 kcal/mol). Overall, our computed mechanism is in good agreement with experimental ^{1}H NMR observations, which reveal no detectable yield of the monoborylimine intermediate, thereby supporting the rapid and sequential double hydroboration leading directly to the diborylamine product.

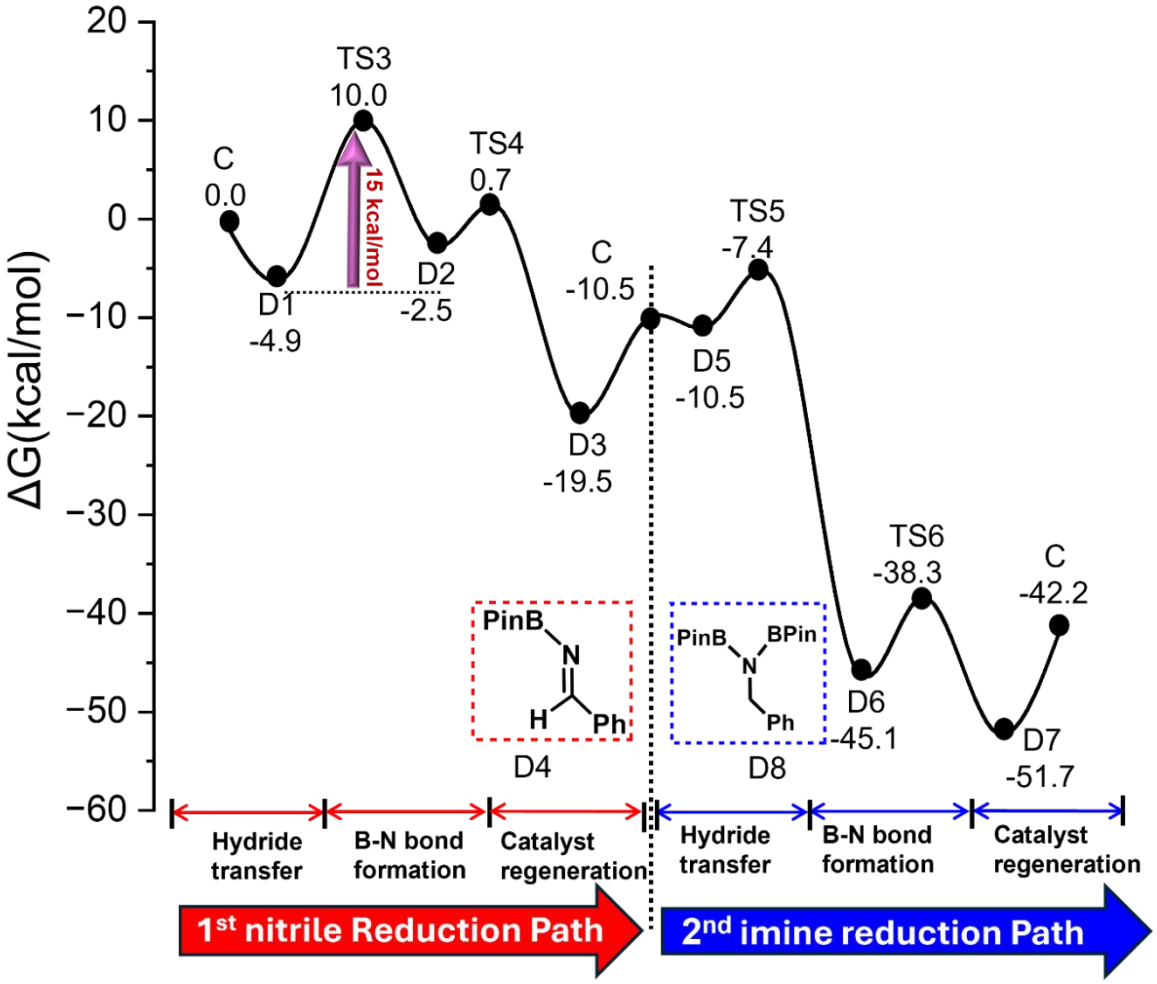

Fig. 4. DLPNO-CCSD(T)/def2-TZVPP//M06/6-31G** computed relative Gibbs free energy profile for the neosilyllithium-catalyzed dihydroboration of phenyl nitrile. The relative free energy of each intermediate and transition state is given in kcal/mol.

Hydroboration of Aldehydes and Esters

Next, we analyzed the mechanism of the hydroboration for aldehyde and ester compounds, where benzaldehyde **(E)** and methyl benzoate **(F)** were used as substrates. For aldehyde hydroboration, the

View Article Online
DOI: 10.1039/D5CP02589C

reaction cycle initiates with binding the carbonyl oxygen lone pair of substrate **E** to the lithium atom of the active catalyst **C**, forming an intermediate **E1**. The binding of substrate results in the slight elongation of the C=O bond and stabilizes species **E1** by ~6.2 kcal/mol compared to the non-interacting species. In the next step, the B-H bond breaks, and a hydride transfer occurs from the B atom to the sp^2-hybridized carbon atom of the benzaldehyde, forming the intermediate **E2**, which is stabilized by ~16.5 kcal/mol compared to **E1**. This step occurs via the six-membered transition state **TS7** with a free energy barrier of ~ 8.2 kcal/mol. The computed C=O bond length elongation in **TS7** confirms the reduction of the aldehyde, consistent with hydride transfer into the carbonyl π* orbital. In the subsequent step, the Li-O bond is likely to break and allow the migration of the alkoxy group to the boron centre, and later, the HBPin flushes out the BPin-CH_2O as the desired product and regenerates the catalyst C for the subsequent cycle. Despite a rigorous search, we could not locate the transition state related to the breaking of the Li-O bond and migration of the alkoxy group to the boron centers. All our TS search leads to the formation of the intermediate **E3**, where the O atom of the alkoxide is coordinated with the Li and boron, and one O atom of the HBPin comes in one plane and forms a four-membered ring. (see Fig. 5a) This rearrangement occurs through a low-energy barrier transition state, **TS8** of 3.0 kcal/mol. Notably, the **E2→TS8→E3** process is highly exergonic, where species **E3** is stabilized by ~16.4 kcal/mol compared to the preceding intermediate despite having a strained four-membered ring. A strong ionic interaction between the $B^{\delta+}$---$O^{\delta-}$ bond of the zwitterionic intermediate and the $Li^{\delta+}$---$O^{\delta-}$ bond offers a significant stabilization to the **E3** intermediate despite the formation of the strained four-membered ring. It is evident from the computed energetics (see Fig. 5b and 5c) that the breaking of the Li-O bond in **E3** is a highly endergonic process, and the subsequent conversion of **E3** to the final product requires enormous free change, rendering this pathway unfavourable. Our computed pathway (path I) represents the case where one mole of HBPin is involved in the reaction. Next, we explored an alternative pathway (path II) where the species **E3** first undergoes ligand exchange with the HBPin, releases CH_2SiH_3-Bpin, and generates species **E5**, which is destabilized by ~5 kcal/mol compared to the preceding intermediate **E3**. After the formation of **E5**, a second molecule of benzaldehyde coordinates to the lithium center, leading to the formation of intermediate **E6**, which is further stabilized by ~8.6 kcal/mol relative to **E5**. Notably, the lithium center remains coordinated to two oxygen atoms

throughout the process, maintaining the structural integrity of the four-membered ring. The incoming benzaldehyde approaches from the sterically accessible, open face of lithium and binds via its carbonyl oxygen, enabling a favorable Li···O interaction. This coordination significantly enhances the stability of **E6** by reinforcing lithium–oxygen interactions and optimizing the overall geometry of the complex. Furthermore, the presence of the tetracoordinated boron centre of HBPin in intermediate **E6** allows facile hydride transfer from the boron centre to the coordinated benzaldehyde molecule via **TS9**. This transition state requires a free energy barrier of ~11.7 kcal/mol to form species **E7**. The species **E7** is stabilized by ~ 20 kcal/mol compared to **E6**. Compared to the previous pathway, which is a highly endergonic process due to the energetic penalty associated with breaking the Li-O bond **(E3** to **E4)**, the involvement of two moles of substrate and HBPin leads to the facile hydride transfer, which is the key step for the hydroboration of aldehydes. This pathway avoids breaking the stable Li–O bond, which helps lower the overall energy required for the reaction. Finally, the desired product $PhCH_2OBPin$ (**E8**) is formed through a ligand exchange step with HBPin, which simultaneously regenerates **E5** for the next catalytic cycle. Comparative mechanistic studies indicate that path II is likely to be energetically more favorable for the hydroboration of the aldehydes. The computed path II matches the previously reported Bao's mechanism proposed for n-BuLi-catalysed hydroboration of the benzaldehydes [38]

View Article Online
DOI: 10.1039/D5CP02589C

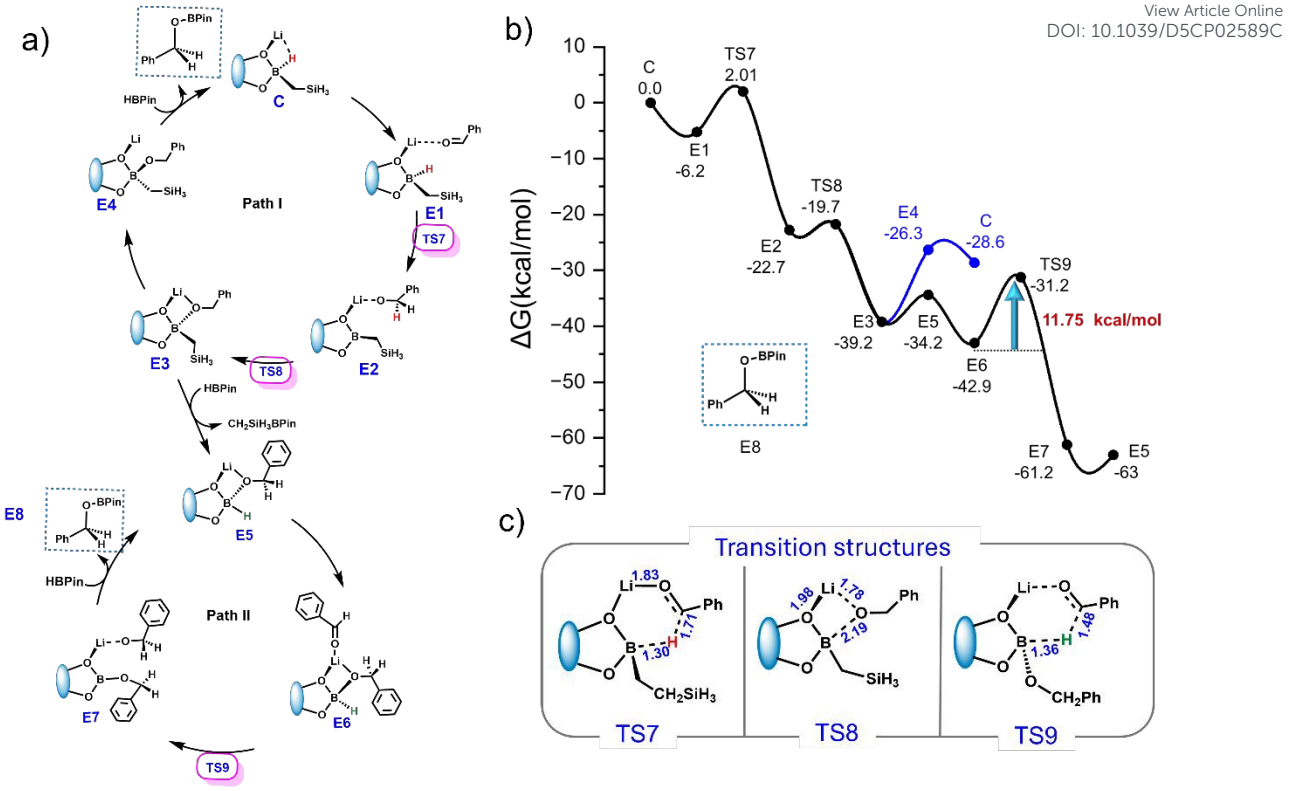

Fig. 5: **a)** Proposed catalytic cycle for neosilyllithium-catalyzed hydroboration of benzaldehyde (E) **b)** DLPNO-CCSD(T)/def2-TZVPP//M06/6-31G** computed relative Gibbs free energy profile for the neosilyllithium-catalyzed hydroboration of benzaldehyde. The relative free energy of each intermediate and transition state is given in kcal/mol. **c)** Transition structures with important hydrogen atoms shown for clarity. DFT-computed bond lengths are given in Å.

A similar hydroboration strategy can be extended to esters, wherein the carbonyl group undergoes reduction via a hydride transfer mechanism. However, the hydroboration of esters stands out from other carbonyl compounds due to its tendency to yield a mixture of alcohol products. Experimental observations show the neosilyllithium catalyzed hydroboration of ester yields a mixture of alcohols ($PhCH_2OBPin$ + CH_3OBPin), indicating no aldehyde was obtained as a result of partial reduction.[72]. Here we employed methyl benzoate **(F)** as the substrate, where hydroboration is expected to generate a mixture of alcohols ($PhCH_2OBPin$ + CH_3OBPin), which requires two reduction events, where the first reduction leads to the formation of an aldehyde and the second reduction generates alcohols. In the initial step, the catalyst **C** undergoes a ligand exchange with one equivalent of HBPin, which flushes out the BPin–CH_2SiH_3 species, resulting in the formation of intermediate **F1,** which is stabilized by

~2.2 kcal/mol relative to species **C**. The formation of species **F1** is necessary as two hydride atoms attached to the boron center are required for the hydride migration and generation of two alcohols. In the next step, methyl benzoate **(F)** coordinates with the intermediate **F1** and forms an intermediate **F2**, which is stabilized by ~5.5 kcal/mol relative to the unreacted species (see Fig. 6). DFT optimized geometry of **F2** shows a slight elongation (~0.02 Å) in the carbonyl bond (C–O_a bond) while the methoxy C–O_b bond becomes relatively shorter (1.345 Å to 1.316 Å) compared to unreacted species. Next, the hydride transfer takes place from dihydridoborane to the *sp²* hybridized C atom (C–O_a bond) of the coordinated ester through a six-membered transition state (**TS10**) to yield an intermediate **F3,** which is ~3.5 kcal/mol stabilized compared to the preceding intermediate **F2**. The **TS10** requires an activation energy barrier of ~17.4 kcal/mol for the hydride transfer. In the **TS10**, the key C-O_a/B-H/C-H bond lengths are 1.271 Å /1.375 /1.493 Å, respectively, indicating that the breaking of the C=O and B-H bond occurs simultaneously with the formation of the C-H bond. This highly concerted and facile hydride transfer mainly arises due to the nearly coplanar arrangement of all six atoms (Li, O, B, H, C, O_a) participating in the bond cleavage/formation. Second-order perturbation analysis shows an interaction of ~ 200 kcal/mol from the (B-H) bonding orbital to the antibonding π* orbital of the C=O_a, which helps in reducing the C=O_a double bond. At the same time, the C–O_b bond length increases to ~1.42 Å in **F3** (~ 0.1 Å increased compared to the **F2** intermediate), which hints that the weak C–O_b bond length is likely to break in the next step and migrate to the electron-deficient boron center. The migration of the methoxy group from the ester carbon to the boron center occurs via a low-barrier four-membered transition state **TS12** ($\Delta G^{\ddagger}$ = *1.3 kcal/mol*), and generates an intermediate zwitterionic intermediate **F4**, which is stabilized by ~10.49 kcal/mol compared to preceding intermediate **F3**. In the next step, the second hydride transfer takes place from the boron centre to the *sp²* hybridized carbon atom of the C=O_a moiety via a six-membered transition state (**TS12**) to yield species **F5**, which is stabilized by 19.6 kcal/mol than the preceding intermediate **F4.** The activation energy barrier corresponding to **TS12** is ~8.9 kcal/mol for the second hydride transfer, ~50% of the first hydride transfer occurring through the **TS10.** In the final transformation, a rapid transfer of the -CH_2Ph group (benzyl group) to the boron centre of HBPin occurs through a four-membered transition state (**TS13**), with a relatively low activation barrier of ~4.1 kcal/mol, yielding an intermediate **F6**. Finally, the

View Article Online
DOI: 10.1039/D5CP02589C

presence of excess HBPin promotes the formation and release of the reduction products $PhCH_2OBPin$ (**F7**) and CH_3OBPin (**F8**) and restores the active dihydride complex **F1**, completing the catalytic cycle and enabling further turnovers. DFT calculations predict the first hydride transfer via **TS10** (*$\Delta G^{\ddagger}$ = ~17.4 kcal/mol*) to be the rate-determining step in the hydroboration of esters.

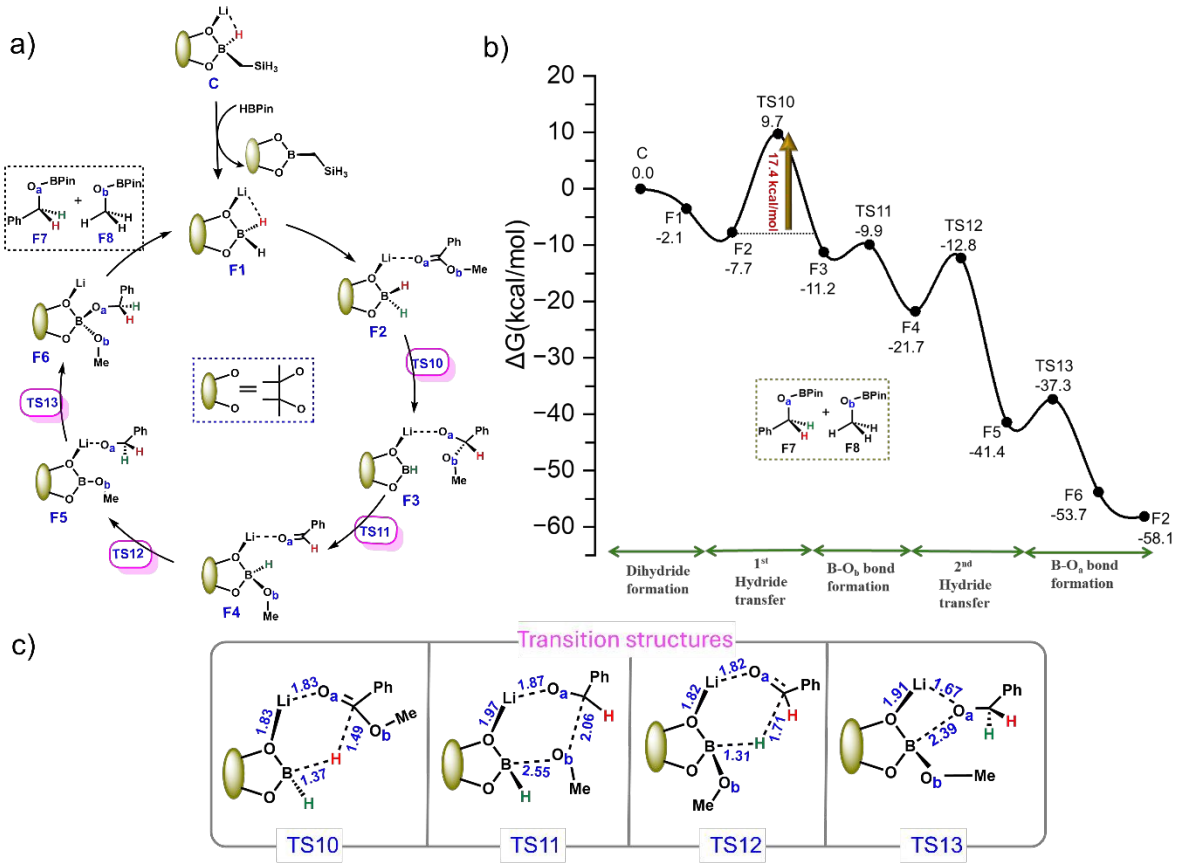

Fig. 6: **a)** Proposed catalytic cycle for neosilyllithium-catalyzed hydroboration of methyl benzoate (F); **b)** DLPNO-CCSD(T)/def2-TZVPP//M06/6-31G** calculated relative Gibbs free energy profile for the neosilyllithium-catalyzed hydroboration of methyl benzoate (**F**). The relative free energy of each intermediate and transition state is given in kcal/mol. **c)** Transition structures with important hydrogen atoms are shown for clarity. Bond lengths (in blue) are given in Å.

It is evident from the computed thermodynamic reaction profile that the rate-determining step for ester hydroboration is mainly the first hydride transfer, which occurs through a high energy barrier **TS10** (*$\Delta G^{\ddagger}$ = 17.5 kcal/mol*) compared to the second hydride transfer via **TS12** (*$\Delta G^{\ddagger}$ = 8.9 kcal/mol*), where the aldehyde get reduced to the alcohol. Moreover, the rate-determining step for hydroboration of benzaldehyde is **TS9** (*$\Delta G^{\ddagger}$ =11.7 kcal/mol*), which is also much lower than the first hydride transfer that occurs in the case of ester hydroboration. DFT computed reaction profile indicates that reducing

View Article Online
DOI: 10.1039/D5CP02589C

the C=O bond in esters (-COOMe) is much more challenging than that of aldehydes (-CHO), which aligns with experimental observations.[17,30,35] To understand the origin of the difference in the hydride transfer pathway, we conducted an activation strain analysis (ASA) calculation on the transition states **TS10** (ester) and **TS12** (aldehyde). Here, we fragmented the transition state into two parts: (i) the catalyst core and (ii) the substrate, and then computed the overall interaction energy ($\Delta E^{\ddagger}$) in the form of geometric distortion energy (ΔE_{dist}) and interaction energy (ΔE_{int}), where the ΔE_{dist} represents the energetic penalty associated with deforming the fragments from their equilibrium geometries to those in the transition state, while the ΔE_{int} captures stabilizing or destabilizing interactions between the distorted fragments (see Fig. 7). In the early part of the reaction coordinate, the strain energy remains minimal, suggesting that both the catalyst and substrate retain their near-equilibrium geometries. As the system approaches the transition state, which is indicated by the C-H bond stretch, we see that the strain energy increases in both situations; however, the magnitude of the increase is significantly greater in the case of the ester. This sharp increase in ΔE_{dist} value is mainly attributed to significant steric repulsion between the bulky alkoxy group of the ester and the catalyst core. On the other hand, the strain energy is nearly ~2x times smaller for the **TS12** due to the reduced steric hindrance between the PhCHO and the catalyst core. As a result of the stronger Li…O electrostatic interactions, the ΔE_{int} value is much larger for **TS10** (–9.7 kcal mol^{-1}) compared to **TS12** (–4.1 kcal mol^{-1}), which is reflected in the steeper descent of the ΔE_{int} curve for the **TS10**. This stronger interaction not only helps to lower the activation energy barrier but also shifts the **TS10** to an earlier position along the reaction coordinate compared to **TS12**. Despite having a favorable interaction energy, the high strain energy associated with steric factors dominates in esters, which results in a significant activation energy barrier for the hydride transfer compared to the aldehydes. Overall, the ASA calculations highlight that steric effects dominate over electronic factors in determining the reactivity trends, explaining the sluggish hydroboration of esters relative to aldehydes.

View Article Online
DOI: 10.1039/D5CP02589C

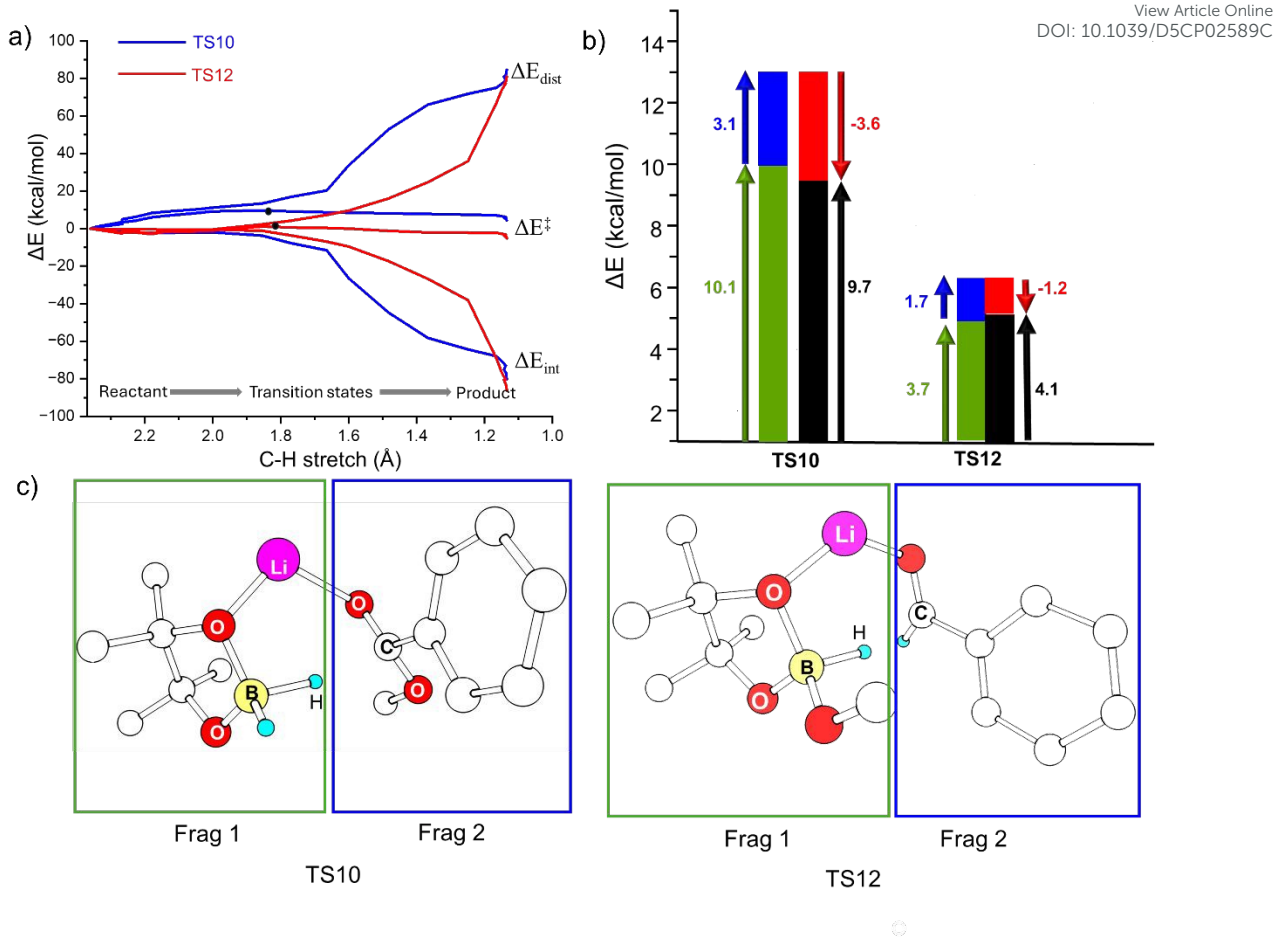

Fig. 7: **a)** ASA plots showing the decomposition of activation energy into strain energy (ΔE_{dist}) and interaction energy (ΔE_{int}) for the transition states TS11 (ester, blue) and TS13 (aldehyde, red) **b)** Bar diagram representation of the total activation energy (black arrow), strain energy (green), and interaction energy (red). **c)** Optimized geometries of TS10 (left) and TS12 (right), shown as two parts: Fragment 1 (green) includes the boron unit, and Fragment 2 (blue) shows the coordinated substrate.

Conclusion

In this study, we have elucidated the detailed mechanistic pathways of neosilyllithium-catalyzed hydroboration of nitrile, aldehyde, and ester using high-level DLPNO-CCSD(T) calculations, aiming to uncover the origins of its substrate-dependent reactivity. In the absence of a catalyst, hydroboration of nitriles and aldehydes proceeds via prohibitively high-energy four-membered transition states ($\Delta G^{\ddagger} > 40$ *kcal mol*$^{-1}$), making these transformations unfeasible under mild conditions. However, activation

View Article Online
DOI: 10.1039/D5CP02589C

of HBPin by neosilyllithium generates a zwitterionic intermediate that effectively polarizes the B–H bond, allowing a much more accessible hydride transfer to occur. Across all substrates, the catalytic cycle follows a common pathway: hydride transfer from the boron center to the electrophilic carbon (carbonyl or nitrile), followed by migratory insertion into the boron center, highlighting the dual role of HBPin as hydride transfer agent and functional group acceptor. The catalytic cycle for nitriles proceeds via a two-step hydride transfer pathway, with the first step—conversion of the nitrile to an imine—identified as the rate-determining step, followed by a much faster second reduction to yield the diborylamine product. DLPNO-CCSD(T) computed reaction profile suggests a sequential double reduction of the nitrile, which leads to the diborylated product, which agrees with experimental observation. For aldehydes, the hydroboration follows a more straightforward pathway with a moderate hydride transfer barrier (~8.3 kcal/mol) and an energetically favorable catalytic cycle involving two equivalents of substrate. On the other hand, esters present a mechanistic challenge due to their bulkier structure and subtle electronic effects. The first hydride transfer in ester hydroboration requires a much higher activation energy barrier (~17.5 kcal/mol) compared to the second hydride transfer (~8.9 kcal/mol), which reduces the intermediate aldehyde to the mixture of alcohols ($PhCH_2OBPin$ and CH_3OBPin). ASAand EDA analysis show that despite having favourable orbital interactions, a dominant strain energy due to the bulkiness of the ester and catalyst core penalizes the interaction energy, which results in the higher activation energy for the esters compared to the aldehydes. Our results rationalize the experimentally observed reactivity order—aldehydes >> esters—and establish neosilyllithium as a powerful main-group catalyst for the hydroboration reaction of different substrates. Overall, this work provides an in-depth mechanistic insight into the neosilyllithium-catalysed hydroboration reaction and highlights how the electronic and steric effects control the reactivity of the different substrates, and our findings pave the way for designing novel lithium-catalyzed organic transformations.

View Article Online
DOI: 10.1039/D5CP02589C

Author contributions

Mridula Choudhary: Methodology, Data curation, Validation, Writing, **Tarun K. Panda:** Writing – review & editing, **Saurabh Kumar Singh:** Supervision, Conceptualization, Project administration, Writing – review & editing, Funding acquisition.

Data availability

The data supporting this article have been included as part of the ESI.

Conflicts of interest

There are no conflicts to declare.

Acknowledgements

SKS acknowledges the Core Research Grant CRG(2023/002936) for the financial support. M C thanks UGC for the SRF fellowship. The authors also acknowledge the PARAM Seva Computing Facility under the National Supercomputing Mission at the Indian Institute of Technology, Hyderabad.

References

1 H. C. Brown and B. C. S. Rao, *J. Am. Chem. Soc.*, 1956, **78**, 5694–5695.

2 C. C. Chong and R. Kinjo, *ACS Catal.*, 2015, 5, 3238-3259

3 M. L. Shegavi and S. K. Bose, *Catal. Sci. Technol.*, 2019, **9**, 3307–3336.

4 A. Suzuki, *Angew. Chem. Int. Ed.,* 2011, **50**, 6722–6737.

5 Norio. Miyaura and Akira. Suzuki, *Chem. Rev.*, 1995, **95**, 2457–2483.

6 D. Leonori and V. K. Aggarwal, *Angew. Chem. Int. Ed.,* 2015, **54**, 1082–1096.

7 J. Seyden-Penne, Reductions by the Alumino- and Borohydrides in Organic Synthesis, *John Wiley & Sons*, 1997.

8 H. C. Brown, S. Narasimhan and Y. M. Choi, *J. Org. Chem.*, 1982, **47**, 4702–4708.

9 L. Pasumansky, D. Haddenham, J. W. Clary, G. B. Fisher, C. T. Goralski and B. Singaram, *J. Org. Chem.*, 2008, **73**, 1898–1905.

10 Y. Pouilloux, F. Autin and J. Barrault, *Catal. Today*, 2000, **63**, 87–100.

11 H. Kono, K. Ito and Y. Nagai, *Chem. Lett.,* 1975, **4**, 1095–1096.

12 D. Männig and H. Nöth, *Angew. Chem. Int. Ed.*, 1985, **24**, 878–879.

13 K. Nie, Y. Han, C. Wang and X. Cheng, *Appl. Organomet. Chem.*, 2022, **36**, e6570.

14 S. J. Geier, C. M. Vogels, J. A. Melanson and S. A. Westcott, *Chem. Soc. Rev.,* 2022, **51**, 8877–8922.

15 C. J. Barger, A. Motta, V. L. Weidner, T. L. Lohr and T. J. Marks, *ACS Catal.*, 2019, **9**, 9015–9024.

16 S. Saha and M. S. Eisen, *ACS Catal.*, 2019, **9**, 5947–5956.

17 K. Makarov, A. Kaushansky and M. S. Eisen, *ACS Catal.*, 2022, **12**, 273–284.

18 S. Patnaik and A. D. Sadow, *Angew. Chem. Int. Ed.*, 2019, **58**, 2505–2509.

19 M. Magre, M. Szewczyk and M. Rueping, *Chem. Rev.*, 2022, **122**, 8261–8312.

20 A. Das, S. Rej and T. K. Panda, *Dalton Trans.*, 2022, **51**, 3027–3040.

21 S. Rej, A. Das and T. K. Panda, *Adv. Synth. Catal.*, 2021, **363**, 4818–4840.

22 M. Arrowsmith, T. J. Hadlington, M. S. Hill and G. Kociok-Köhn, *Chem. Commun.*, 2012, **48**, 4567–4569.

23 M. Arrowsmith, M. S. Hill and G. Kociok-Köhn, *Chem. -Eur. J.*, 2013, **19**, 2776–2783.

24 D. Mukherjee, S. Shirase, T. P. Spaniol, K. Mashima and J. Okuda, *Chem. Commun.*, 2016, **52**, 13155–13158.

25 L. Fohlmeister and A. Stasch, *Chem. Eur. J.*, 2016, **22**, 10235–10246.

26 S. Yadav, S. Pahar and S. S. Sen, *Chem. Commun.*, 2017, **53**, 4562–4564.

27 S. Yadav, R. Dixit, M. K. Bisai, K. Vanka and S. S. Sen, *Organometallics*, 2018, **37**, 4576–4584.

28 D. Mukherjee, A. Ellern and A. D. Sadow, *Chem. Sci.*, 2014, **5**, 959–964.

29 M. Magre, B. Maity, A. Falconnet, L. Cavallo and M. Rueping, *Angew. Chem. Int. Ed.,* 2019, **58**, 7025-7029

30 X. Zhang, K. Lu, X. Chen, G. Su, X. Rong and M. Ma, *Org. Biomol. Chem.*, 2024, **22**, 5353–5360.

31 R. Kumar, S. Dutta, V. Sharma, P. P. Singh, R. G. Gonnade, D. Koley and S. S. Sen, *Chem. -Eur. J.*, 2022, **28**, e202201896.

32 M. Rauch, S. Ruccolo and G. Parkin, *J. Am. Chem. Soc.*, 2017, **139**, 13264–13267.

33 C. Weetman, M. D. Anker, M. Arrowsmith, M. S. Hill, G. Kociok-Köhn, D. J. Liptrot and M. F. Mahon, *Chem. Sci.*, 2016, **7**, 628–641.

34 C. Weetman, M. S. Hill and M. F. Mahon, *Chem. -Eur. J.* 2016, **22**, 7158–7162.

35 K. Kuciński and G. Hreczycho, *Green Chemistry*, 2020, **22**, 5210–5224.

36 D. Mukherjee, H. Osseili, T. P. Spaniol and J. Okuda, *J. Am. Chem. Soc.*, 2016, **138**, 10790–10793.

37 M. K. Bisai, T. Das, K. Vanka and S. S. Sen, *Chem. Commun.*, 2018, **54**, 6843–6846.

38 Z. Zhu, X. Wu, X. Xu, Z. Wu, M. Xue, Y. Yao, Q. Shen and X. Bao, *J. Org. Chem.*, 2018, **83**, 10677–10683.

39 L. H. Slaugh, *Tetrahedron*, 1966, **22**, 1741–1746.

40 S. Wang, K. Murata, T. Hayakawa, S. Hamakawa and K. Suzuki, *Chem. Commun.*, 1999, 103–104.

41 A. K. Sutar, T. Maharana, S. Dutta, C.-T. Chen and C.-C. Lin, *Chem. Soc. Rev.*, 2010, **39**, 1724–1746.

42 D. Prajapati, K. C. Lekhok, J. S. Sandhu and A. C. Ghosh, *J. Chem. Soc., Perkin Trans. 1*, 1996, 959–960.

43 G. Sai Kumar, J. Bhattacharjee, K. Kumari, S. Moorthy, A. Bandyopadhyay, S. K. Singh and T. K. Panda, *Polyhedron*, 2022, **219**, 115784.

44 G. S. Kumar, S. Moorthy, H. Karmakar, S. K. Singh and T. K. Panda, *Eur. J. Inorg. Chem.*, 2022, e202100895.

45 Frisch, M. J.; Trucks, G. W.; Schlegel, H. B.; Scuseria, G. E.; Robb, M. A.; Cheeseman, J. R.; Scalmani, G.; Barone, V.; Mennucci, B.; Petersson, G. A.; Nakatsuji, H.; Caricato, M.; Li, X.; Hratchian, H. P.; Izmaylov, A. F.; Bloino, J.; Zheng, G.; Sonnenberg, J. L.; Hada, M.; Ehara, M.; Toyota, K.; Fukuda, R.; Hasegawa, J.; Ishida, M.; Nakajima, T.; Honda, Y.; Kitao, O.; Nakai, H.; Vreven, T.; Montgomery, J. A. Jr.; Peralta, J. E.; Ogliaro, F.; Bearpark, M.; Heyd, J. J.; Brothers, E.; Kudin, K. N.; Staroverov, V. N.; Kobayashi, R.; Normand, J.; Raghavachari, K.; Rendell, A.; Burant, J. C.; Iyengar, S. S.; Tomasi, J.; Cossi, M.; Rega, N.; Millam, J. M.; Klene, M.; Knox, J. E.; Cross, J. B.; Bakken, V.; Adamo, C.; Jaramillo, J.; Gomperts, R.; Stratmann, R. E.; Yazyev, O.; Austin, A. J.; Cammi, R.; Pomelli, C.; Ochterski, J. W.; Martin, R. L.; Morokuma, K.; Zakrzewski, V. G.; Voth, G. A.; Salvador, P.; Dannenberg, J. J.; Dapprich, S.; Daniels, A. D.; Farkas, Ö.; Foresman, J. B.; Ortiz, J. V.; Cioslowski, J.; Fox, D. J.; Gaussian, Inc., Wallingford CT, 2009.

46 Y. Zhao and D. G. Truhlar, *Theor. Chem. Acc.*, 2008, **120**, 215–241.

47 Y. Zhao and D. G. Truhlar, *Acc. Chem. Res.*, 2008, **41**, 157–167.

48 Y. Zhao and D. G. Truhlar, *Org. Lett.*, 2007, **9**, 1967–1970.

49 W. J. Hehre, R. Ditchfield and J. A. Pople, *J. Chem. Phys.* , 1972, **56**, 2257–2261.

50 C. Lee, W. Yang and R. G. Parr, *Phys. Rev. B*, 1988, **37**, 785–789.

51 A. D. Becke, *J. Chem. Phys.*, 1993, **98**, 5648–5652.

52 K. Fukui, *Acc. Chem. Res.*, 1981, **14**, 363–368.

53 C. Gonzalez and H. B. Schlegel, *J. Chem. Phys.*, 1989, **90**, 2154–2161.

54 Carlos. Gonzalez and H. Bernhard. Schlegel, *J. Phys. Chem.*, 1990, **94**, 5523–5527.

View Article Online
DOI: 10.1039/D5CP02589C

55 C. Riplinger and F. Neese, *J. Chem. Phys*., 2013, **138**, 034106.

56 C. Riplinger, B. Sandhoefer, A. Hansen and F. Neese, *J. Chem. Phys.*, 2013, **139**, 134101.

57 F. Neese, *WIREs Comput. Mol. Sci.* , 2012, **2**, 73–78.

58 F. Weigend, *Phys. Chem. Chem. Phys.*, 2006, **8**, 1057–1065.

59 F. Neese, *WIREs Comput. Mol. Sci.,* 2022, **12**, e1606.

60 G. Knizia and J. E. M. N. Klein, *Angew. Chem. Int. Ed.*, 2015, **54**, 5518–5522.

61 T. Lu and F. Chen, *J. Comput. Chem.*, 2012, **33**, 580–592.

62 W. Humphrey, A. Dalke and K. Schulten, *J. Mol. Graph*, 1996, **14**, 33–38.

63 A. Diefenbach and F. M. Bickelhaupt, *J. Phys. Chem. A*, 2004, **108**, 8460–8466.

64 F. M. Bickelhaupt, *J. Comput. Chem.*, 1999, **20**, 114–128.

65 W.-J. van Zeist and F. Matthias Bickelhaupt, *Org. Biomol. Chem.*, 2010, **8**, 3118–3127.

66 A. D. Bage, K. Nicholson, T. A. Hunt, T. Langer and S. P. Thomas, *ACS Catal.*, 2020, **10**, 13479–13486.

67 A. Das and T. K. Panda, *ChemCatChem*, 2023, **15**, e202201011.

68 C. Ni, X. Ma, Z. Yang and H. W. Roesky, *ChemistrySelect*, 2022, **7**, e202202878.

69 D. Bedi, A. Brar and M. Findlater, *Green Chemistry*, 2020, **22**, 1125–1128.

70 P. Ghosh and A. J. von Wangelin, *Org. Chem. Front.*, 2020, **7**, 960–966.

71 A. Kaithal, B. Chatterjee and C. Gunanathan, *J. Org. Chem.*, 2016, **81**, 11153–11161.

72 Y. Ding, X. Ma, Y. Liu, W. Liu, Z. Yang and H. W. Roesky, *Organometallics*, 2019, **38**, 3092–3097.

73 J. Bhattacharjee, P. Rawal, S. Das, A. Harinath, P. Gupta and T. K. Panda, *Dalton Trans.*, 2022, **51**, 5859–586767 A. Das and T. K. Panda, *ChemCatChem*, 2023, **15**, e202201011.

The data supporting this article have been included as part of the Supplementary Information.

View Article Online
DOI: 10.1039/D5CP02589C